Received: 19 January 2023 | Revised: 29 March 2023 | Accepted: 23 April 2023

DOI: 10.1111/cas.15836

ORIGINAL ARTICLE

Cancer Science WILEY

Characterization of starvation response-related genes for predicting prognosis in breast cancer

Yuan Wang[1,2] | Shun Gao[1,2] | Yingkun Xu[1] | Zhenrong Tang[1] | Shengchun Liu[1]

[1]Department of Breast and Thyroid Surgery, The First Affiliated Hospital of Chongqing Medical University, Chongqing, China

[2]Laboratory Research Center, The First Affiliated Hospital of Chongqing Medical University, Chongqing, China

Correspondence
Shengchun Liu, Department of Breast and Thyroid Surgery, The First Affiliated Hospital of Chongqing Medical University, Chongqing, China.
Email: liushengchun1968@163.com

Funding information
Doctoral Research Innovation Project of the First Affiliated Hospital of Chongqing Medical University, Grant/Award Number: CYYY-BSYJSCXXM-202213; National Natural Science Foundation of China, Grant/Award Number: 81772979

Abstract

Breast cancer (BRCA) cells typically exist in nutrient-deficient microenvironments and quickly adapt to states with fluctuating nutrient levels. The tumor microenvironment of starvation is intensely related to metabolism and the malignant progression of BRCA. However, the potential molecular mechanism has not been thoroughly scrutinized. As a result, this study aimed to dissect the prognostic implications of mRNAs involved in the starvation response and construct a signature for forecasting the outcomes of BRCA. In this research, we investigated how starvation could affect BRCA cells' propensities for invasion and migration. The effects of autophagy and glucose metabolism mediated by starved stimulation were examined through transwell assays, western blot, and the detection of glucose concentration. A starvation response-related gene (SRRG) signature was ultimately generated by integrated analysis. The risk score was recognized as an independent risk indicator. The nomogram and calibration curves revealed that the model had excellent prediction accuracy. Functional enrichment analysis indicated this signature was significantly enriched in metabolic-related pathways and energy stress-related biological processes. Furthermore, phosphorylated protein expression of the model core gene EIF2AK3 increased after the stimulus of starvation, and EIF2AK3 may play an essential role in the progression of BRCA in the starved microenvironment. To sum up, we constructed and validated a novel SRRG signature that could accurately predict outcomes and may be developed as a therapeutic target for the precise treatment of BRCA.

KEYWORDS
breast cancer, EIF2AK3, mRNA signature, prognostic prediction, starvation response

Abbreviations: 2DG, 2-deoxy-D-glucose; ARGs, autophagy-related genes; AUC, area under the curve; BRCA, breast cancer; CQ, chloroquine; DEGs, differentially expressed genes; DE-SRRGs, differentially expressed starvation response-related genes; EBSS, Earle's balanced salt solution; EMT, epithelial-mesenchymal transition; GO, gene ontology; GRGs, glycolysis-related genes; GSEA, gene set enrichment analysis; HADb, Human Autophagy Database; KEGG, Kyoto Encyclopedia of Genes and Genomes; KM, Kaplan–Meier; LASSO, least absolute shrinkage and selection operator; PCA, principal component analysis; qPCR, quantitative polymerase chain reaction; ROC, receiver-operating characteristic; SRRG, starvation response-related gene; TCGA, The Cancer Genome Atlas; TME, tumor microenvironment; TNBC, triple-negative breast cancer; WB, western blot.

1 | INTRODUCTION

Breast cancer (BRCA) is a considerably common malignancy in women worldwide.[1] It is critical to gain better insight into the novel and cost-effective prognostic biomarkers to prognosticate and screen the high-risk population with a worse prognosis, advance new therapeutic approaches, and provide timely targeted intervention for BRCA.

The rapidly dividing tumor always exceeds the nutrition reserve, resulting in an adverse tumor microenvironment (TME) characterized by glucose deprivation and amino acid deficiency. The ability to adapt to the harsh TME is critical for cancer cells' survival. Most malignancies, including BRCA, could maximize resource usage to withstand the TME of the nutrient shortage.[2,3] Interfering with the adaptive response may become a novel and practical therapeutic approach since BRCA cells are constantly exposed to and adapted to fluctuating resource supplies.[4]

Energy deficiency may boost autophagy and alter the metabolic pattern of neoplastic cells.[5] Tumor cells adaptively upregulate vital metabolic enzymes of the glycolytic pathway to ensure energy supply during nutrient deprivation.[6] However, research into the molecular mechanisms of BRCA cell survival and progression in starved TME remains limited. Therefore, this study aimed to determine the starvation response-related genes (SRRGs) in BRCA, which could provide valuable insight into the molecular and signaling pathways of energy stress as well as function as biomarkers to predict the survival of BRCA.

In this study, we constructed a starvation response-related gene (SRRG) signature by combining autophagy-related SRRGs and glycolysis-associated SRRGs. This model presents satisfactory predictive accuracy for the predicted outcome and may provide a molecular mechanism for the starved TME involved in BRCA progression. We realized that the stimulus of starvation could provoke autophagy and glucose metabolism reprogramming, which, in turn, increased the epithelial-mesenchymal transition (EMT) in BRCA cells, and the core gene of this model, EIF2AK3, may play a crucial part in its mechanism.

2 | MATERIALS AND METHODS

2.1 | Data acquisition

RNA sequences and clinicopathological information from BRCA were retrieved from the Cancer Genome Atlas (TCGA) database. The study complies with the TCGA data access policy and publication guidelines. Figure 1 presents the flow diagram of the study.

2.2 | Identification of starvation response-related genes

First, SRRGs were obtained from gene set enrichment analysis (GSEA) "GOBP RESPONSE TO STARVATION" in the Molecular Signatures Database (mSigDB).

Second, 232 autophagy-related genes (ARGs) were obtained from the Human Autophagy Database (HADb). Pearson's correlation coefficients were computed to define the correlation between the expression of ARGs and SRRGs. SRRGs linked to autophagy were screened by the standards of $p < 0.001$ and $|r| > 0.3$.

Third, 326 glycolysis-related genes (GRGs) were obtained from the gene sets of mSigDB. Pearson correlation analysis was also used to filter out the SRRGs that are associated with glycolysis based on the criterion of $p < 0.001$ and $|r| > 0.3$.

Finally, we took the intersection between the SRRGs linked to autophagy and the SRRGs associated with glycolysis. The genes at the intersection were designated as candidate SRRGs for further study.

2.3 | Construction and validation of the starvation response-related gene signature

The R "limma" package was employed to screen the differentially expressed genes (DEGs) among tumor and malignant samples from the candidate SRRGs with a false discovery rate <0.05 and a $|\log2FC| > 1.0$. Through univariate regression analysis, the candidate differentially expressed SRRGs (DE-SRRGs) that correlated with overall survival (OS) in the training cohort were identified. Subsequently, the candidate genes were subjected to lasso and stepwise multivariate Cox regression analysis to determine their contribution as independent prognostic elements for OS. Finally, these prognostically DE-SRRGs constituted the prognostic signature.

Based on the expression of SRRGs in the signature and the accompanying regression coefficients, the risk score of each sample was computed utilizing the following formula:

$$\text{Risk score} = \sum_{i=1}^{n} \text{Coef}(i) \times (\text{expression of mRNA}(i)).$$

Samples were allocated to either the lower-risk or higher-risk clusters based on the median value of the risk score. Principal component analysis (PCA) was employed to bunch the samples based on the risk score. OS rates were evaluated by Kaplan–Meier (KM) analysis and compared using the log-rank test. Time-dependent receiver-operating characteristic (ROC) curve analysis was conducted to estimate the prognostic precision of the SRRG signature.

2.4 | Establishment of the nomogram

The nomogram was made to visualize the 3- and 5-year OS in BRCA. The accuracy of the prediction of the SRRG signature was tested by calibration curves.

2.5 | Establishment of the coexpression networks

To visualize the relationship between SRRGs and their associated ARGs or GRGs, coexpression networks were depicted using Cytoscape (3.9.0).

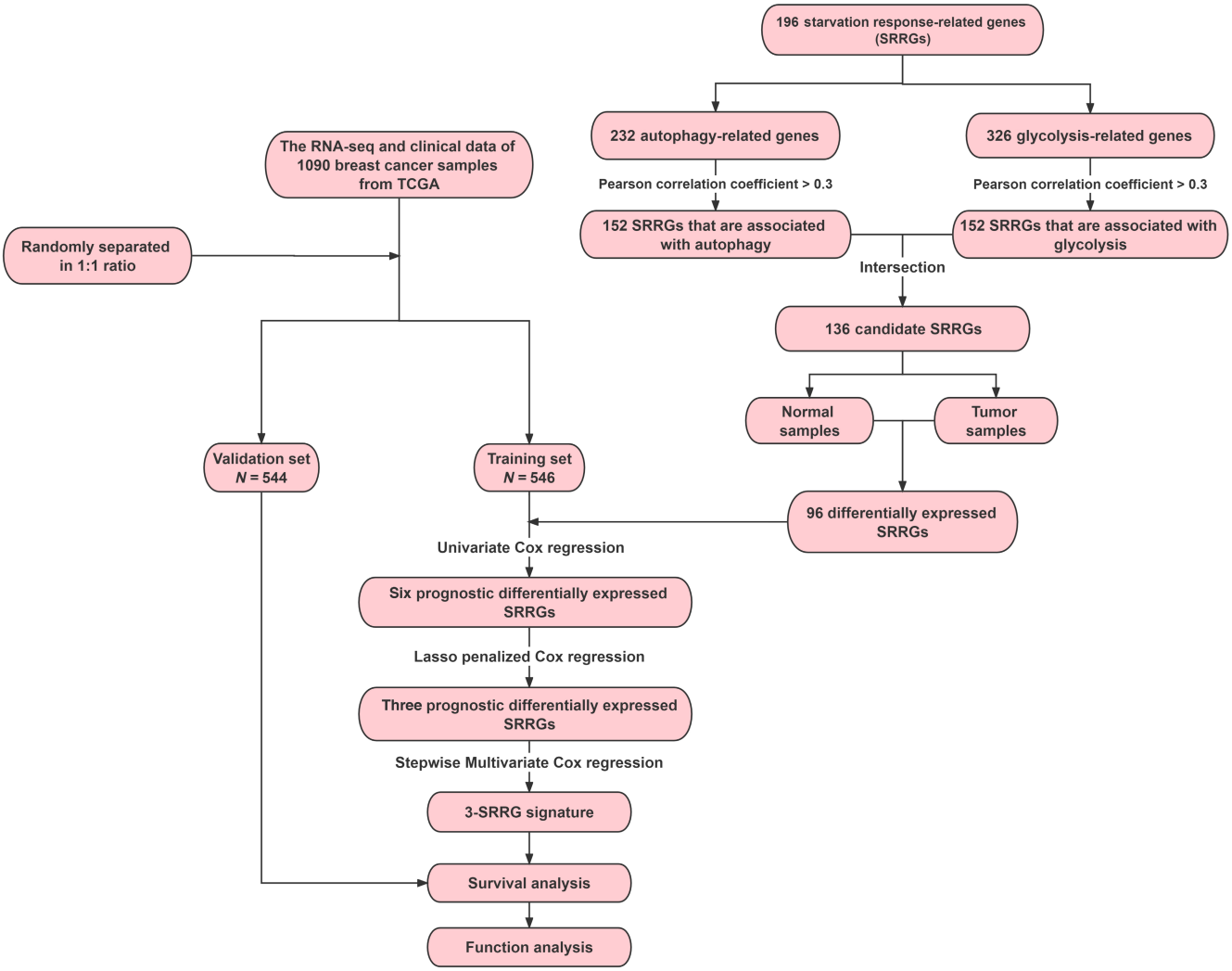

FIGURE 1 Flow chart of the study.

2.6 | Gene set enrichment analysis

The molecular and biological disparities among the higher-and lower-risk groups were investigated employing GSEA (4.3.0).

2.7 | Functional enrichment analysis

Gene ontology (GO) enrichment analysis[7] was carried out to discover the biological processes, molecular functions, and cellular components associated with the SRRG signature. Meanwhile, the signaling pathways considerably enriched by this signature were specified by the Kyoto Encyclopedia of Genes and Genomes (KEGG) enrichment analysis.[8]

2.8 | Cell culture

MDA-MB-231 cell lines were cultured in DMEM supplemented with 10% fetal bovine serum (FBS). BT549 cell lines were cultivated in RPMI 1640 supplemented with 10% FBS. The cells were exposed to Earle's balanced salt solution (EBSS, Solarbio) for 6 h to simulate the starved microenvironment. Cells were all incubated in a 5% CO_2 atmosphere at 37°C.

2.9 | Patients and samples

Paired human clinical specimens originated from BRCA patients at the First Affiliated Hospital of Chongqing Medical University. The study was approved by the Ethics Committee of Chongqing Medical University, and all patients signed informed consent forms.

2.10 | Quantitative polymerase chain reaction

Total RNA was isolated with the Cell Total RNA Isolation Kit (Foregene). RNA was reverse transcribed to cDNA utilizing the RT Master Mix for qPCR II (MedChemExpress). Quantitative polymerase chain reaction (qPCR) was performed with SYBR Green qPCR

Master Mix (MedChemExpress) on a Bio-Rad CFX96 real-time fluorescent quantitative PCR system. The data were standardized to β-actin using the $2^{-\Delta\Delta C_t}$ method. Table S1 lists the primer sequences in detail.

2.11 | Western blot

Total protein was extracted with RIPA lysis buffer (Beyotime), which added protease and phosphatase inhibitors. The protein concentration was detected using the BCA protein detection kit (Beyotime). Equivalent proteins were isolated on 8% or 12% SDS-PAGE gels and then transferred to polyvinylidene fluoride membranes (Millipore). After blocking with 5% bovine serum albumin for 1 h, the membranes were subsequently incubated using primary antibodies overnight at 4°C. The membranes were then incubated with the secondary antibody at 37°C for 1 h and developed with ECL luminescent agent. Antibody names and catalog numbers are described in Table S2.

2.12 | Small interfering RNA transfection

The small interfering RNA (siRNA) was purchased from Tsingke Biotechnology. Cells were transfected with EIF2AK3 siRNAs at a concentration of 50 nM for 6 h. After 48 h, the treated cells were collected for subsequent functional experiments. The sequences of EIF2AK3 siRNAs are detailed in Table S1.

2.13 | Transwell migration and invasion assays

In the upper cavity of 24 well plates, cells were re-suspended in EBSS at a density of 5×10^4 cells per well. Chloroquine (CQ, 20 mM; MedChemExpress) or 2-deoxy-D-glucose (2DG, 5 mM; Selleck Chemicals) was added to the upper chamber as needed for the experiment. The complete medium (CM) was placed in the lower chamber. As controls, cells were seeded in the upper chamber with CM. Chambers were incubated for 12 h. The migration and invasion ability was considered by computing the quantity of migrated cells.

2.14 | Glucose consumption analysis

Glucose consumption was determined after 6 h of cultivation by gauging the concentrations with the commercial kits (Nanjing Jiancheng Biotech) and following the protocols.

2.15 | Immunofluorescence assay

Cells were fixed for 30 min. After permeabilizing with 1% Triton X-100, a primary antibody, rabbit anti-phospho-EIF2AK3 (Thr982) (Abmart), was added. The secondary antibody, Dylight 488, goat anti-rabbit IgG (Abbkine), was then added. After counterstaining with DAPI (Beyotime), cells were observed under a confocal microscope.

2.16 | Statistical analysis

Data were processed using Perl (5.30.0). Statistical analyses were performed utilizing R (4.1.1), SPSS (25.0), and GraphPad Prism (8.0). Pearson correlation coefficients were applied to analyze the correlation between the expression of SRRGs and ARGs or GRGs. The χ^2-test or Mann–Whitney *U*-test was used to examine differences in the proportions of clinicopathological characteristics. Unpaired student *t*-tests were utilized to examine the differences between the two groups. All experiments were conducted at least three times. $p<0.05$ was considered statistically significant ($^*p<0.05$, $^{**}p<0.01$, and $^{***}p<0.001$).

3 | RESULTS

3.1 | Autophagy and glucose metabolism induced by starvation stimulation promote the invasion and migration of breast cancer cells

The BT549 and MDA-MB-231 cells were starved with EBSS for 6 h to simulate the starved microenvironment. Figure 2A,B indicates the capacity for migration and invasion was significantly promoted compared to the culture of the CM.

To ascertain the impact of EBSS on autophagy in BRCA cells, we scrutinized the degree of autophagy by detecting the accumulation of LC3B-II and the degradation of P62. Figure 2C,D indicated that EBSS enhances autophagic flux in BRCA cells. Then, we conducted transwell assays to probe the impact of autophagy induced by starvation stimulation on the invasiveness and metastasis of BRCA cells. In comparison to the standard group or cells additionally processed with CQ, the invasion and migration capacities of BRCA cells were significantly enhanced following only EBSS (Figure 3A and Figure S1A). The above results demonstrated that the autophagy caused by starvation stimulation could encourage the invasion and migration of BRCA cells.

In addition, it has been found that tumor cells respond to the lack of resources by altering glucose uptake and metabolism to maintain energy supply.[6] Therefore, we measured the glucose uptake rate to reflect the extent of glucose metabolism. As illustrated in Figure 2E,F, after the starvation stimulus, both BT549 and MDA-MB-231 cells revealed more elevated levels of glucose uptake, and the co-treatment of EBSS with 2DG could inhibit glucose uptake to some extent. Then, EBSS treated alone most significantly improved the invasive and migratory capacity of BRCA cells when compared to CM or EBSS plus 2DG (Figure 3B and Figure S1B). The above

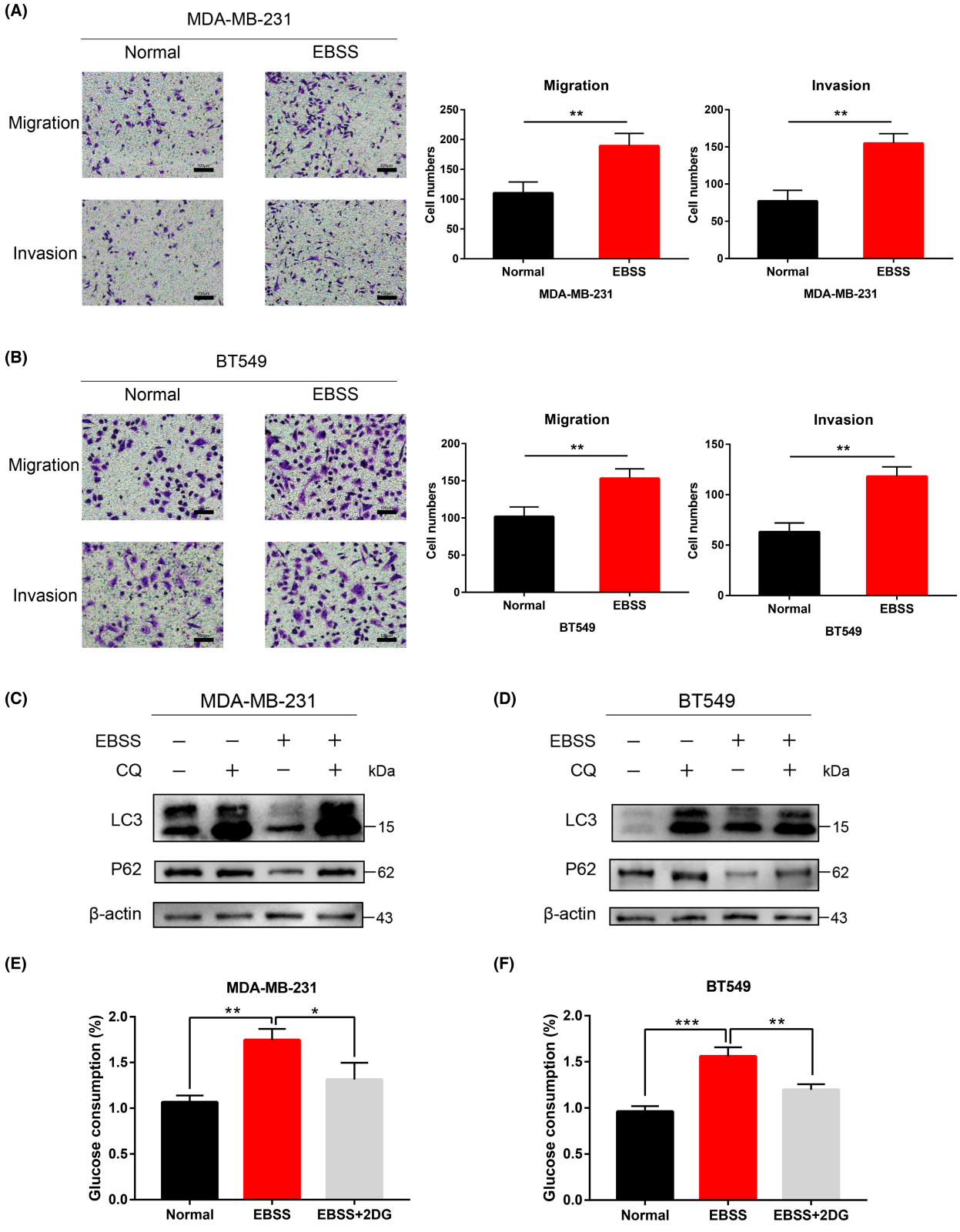

FIGURE 2 Starvation of the microenvironment enhances the progression of breast cancer (BRCA) cells. (A, B) Transwell assays showed the migration and invasion of BRCA cells. Cells were cultured under normal or Earle's balanced salt solution (EBSS) for 6 h before being harvested for transwell assays. The scale bar represents 100 μm. (C, D) Western blot showed the effect of EBSS on autophagy in BRCA cells. (E, F) Glucose consumption ratios were measured.

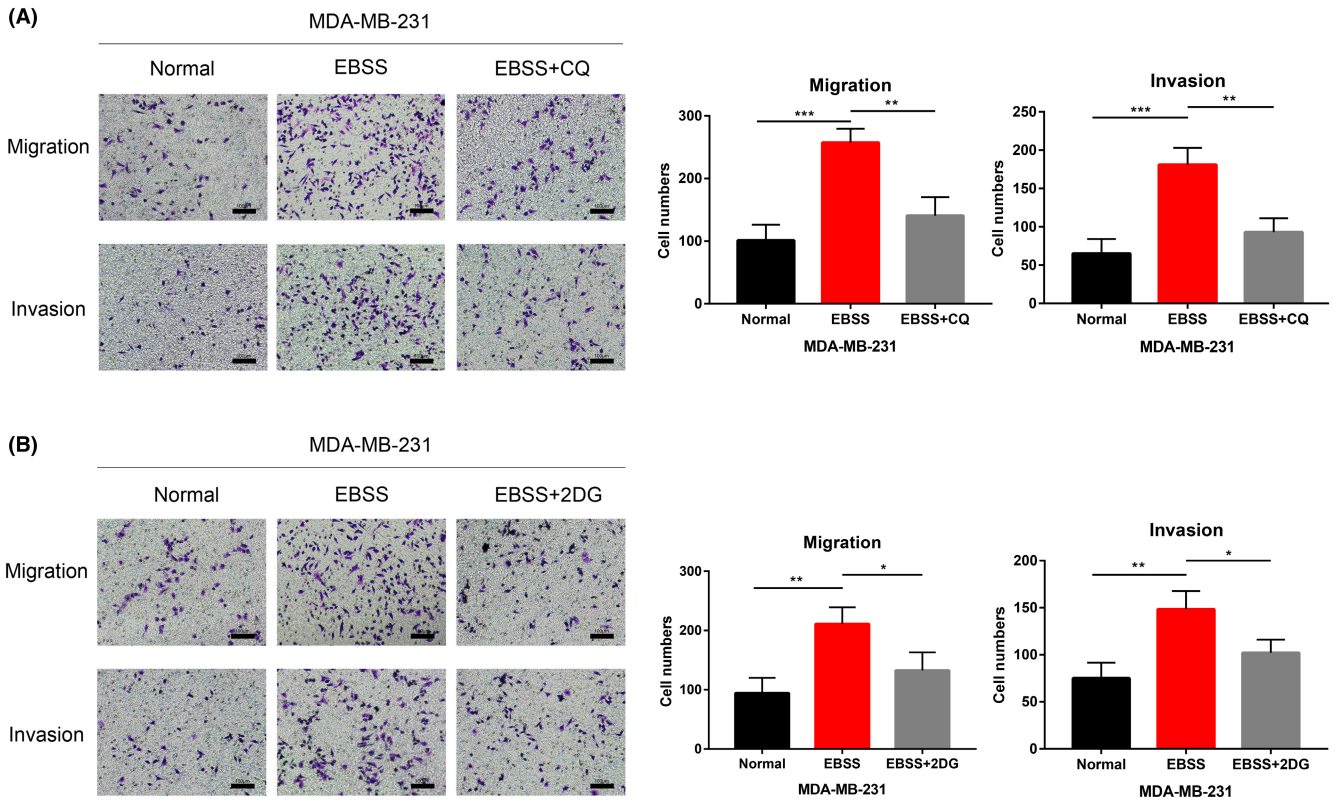

FIGURE 3 Autophagy and glucose metabolism induced by starvation stimulation promote the invasion and migration of MDA-MB-231 cells. (A) Transwell assays showed the effects of autophagy induced by starvation on the migration and invasion of MDA-MB-231 cells. The scale bar represents 100 μm. (B) Transwell assays showed the impact of glycolytic metabolism induced by starvation on the migration and invasion of MDA-MB-231 cells. The scale bar represents 100 μm.

results recommended that the upregulated glucose metabolism induced by starvation stimulation could enhance BRCA's invasive and metastatic potential.

3.2 | Identification of starvation response-related genes in breast cancer

The SRRGs set was obtained from GSEA "GOBP RESPONSE TO STARVATION" in the mSigDB. It incorporated 196 mRNAs responsible for the changes in the behavior of the cell or organism due to the starvation trigger (Table S3).

To begin with, given the fact that starvation stimuli could augment autophagy in BRCA cells, we explored the SRRGs that are associated with autophagy. A total of 232 human ARGs were extracted from HADb (Table S4). According to the coexpression relationship between the expression profile of ARGs and the 196 SRRGs, 152 genes were recognized as the SRRGs associated with autophagy (Table S5). Then, since the above fact indicates that starvation enhanced the glucose consumption of BRCA cells, which mainly tend to operate the glycolytic pathway for fuel generation, we also probed the SRRGs that are associated with glycolysis in BRCA. A total of 326 GRGs were identified in this study (Table S6). According to the coexpression relationship between the expression of GRGs and the 196 SRRGs, 148 genes were determined to be the SRRGs associated with glycolysis (Table S7). Finally, we took the intersection of the 152 SRRGs associated with autophagy and the 148 SRRGs linked with glycolysis. The intersection resulted in 136 genes, which were identified as candidate SRRGs for further study (Figure 4A and Table S8).

Among the 136 candidate SRRGs, 96 were DEGs between normal and malignant samples (Figure 4B). Taken together, these 96 genes were DE-SRRGs of BRCA (Table S9). We then performed GO and KEGG enrichment analysis on these 96 DE-SRRGs.

Gene ontology enrichment analysis indicated that 96 DE-SRRGs were remarkably enriched in the biological process of reactions in the condition of the cell due to the starvation stimulus, such as response to starvation, response to nutrient levels, cellular response to starvation, cellular response to nutrient levels, cellular response to glucose starvation, response to amino acid starvation, and cellular response to amino acid starvation. They were significantly enriched in autophagy-associated cellular components, such as autophagosome and autophagosome membrane. They were also enriched in metabolism-related molecular functions, such as protein

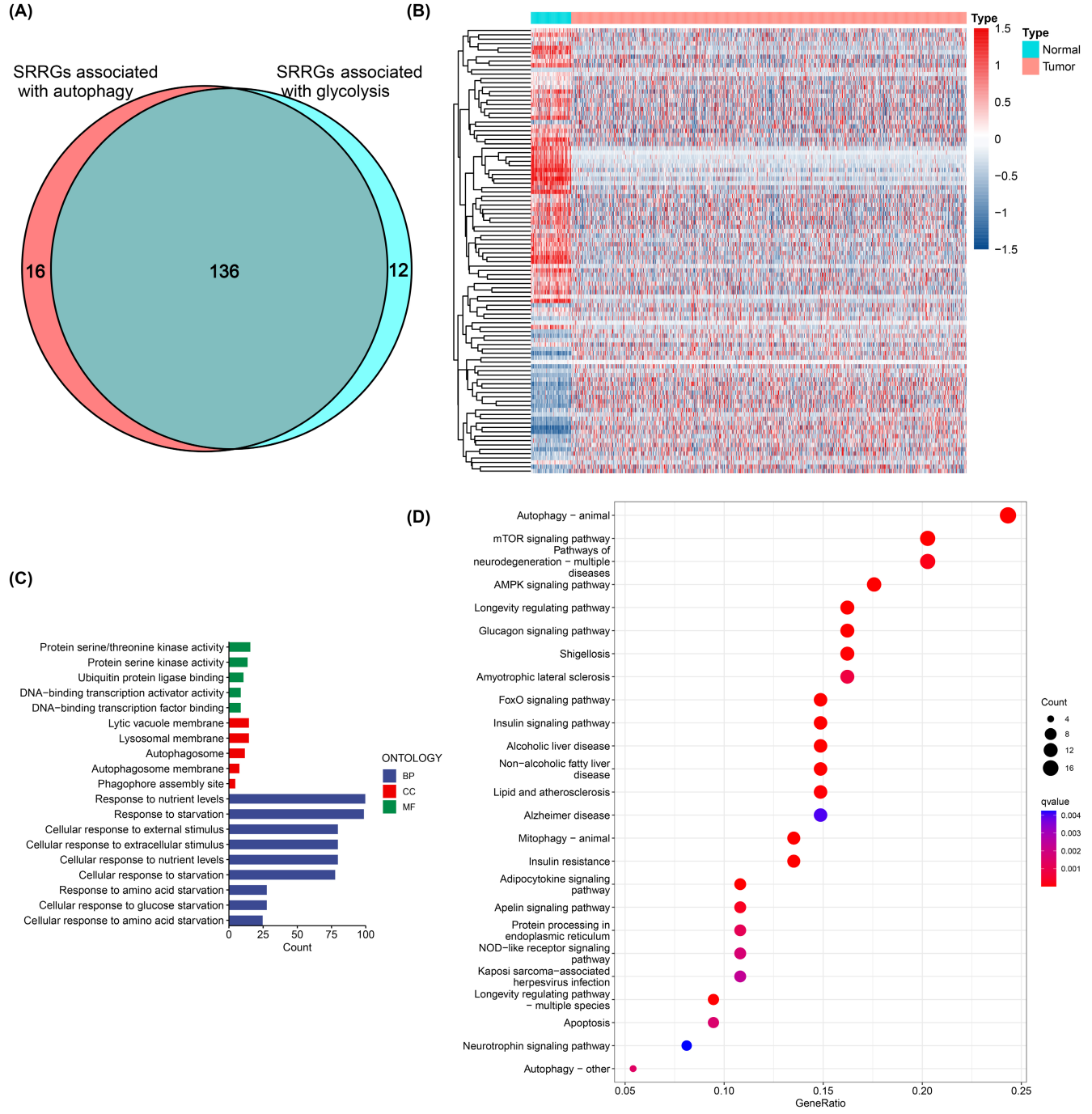

FIGURE 4 Identification of starvation response-related genes (SRRGs) in breast cancer (BRCA). (A) Venn diagram shows the intersection containing 136 candidate SRRGs. (B) Heatmap of the 96 DE-SRRGs. GO (C) and KEGG (D) analysis of the 96 DE-SRRGs. BRCA, breast cancer; DE-SRRGs, differentially expressed SRRGs; GO, gene ontology; KEGG, Kyoto Encyclopedia of Genes and Genomes; SRRG, starvation response-related gene.

serine/threonine kinase activity, protein serine kinase activity, and DNA-binding transcription factor binding (Figure 4C and Table S10). The KEGG pathway analysis revealed that these 96 DE-SRRGs were enriched in energy pressure-related metabolism pathways, including autophagy, mTOR, and AMPK signaling pathways (Figure 4D and Table S11). In short, functional enrichment analyses ascertained that these 96 DE-SRRGs were closely related to starvation response-related metabolism.

3.3 | Construction of the starvation response-related gene signature

A total of 1090 BRCA patients were enrolled in the study. They were randomly assigned to either the training group ($n = 546$) or the validation group ($n = 544$) (Tables S12 and S13). Table 1 illustrates that the proportions of clinicopathological features of patients in the training and validation groups do not differ statistically significantly.

TABLE 1 Clinical characteristics of patients in training and validation cohorts.

Characteristic	Training cohorts (*N* = 546, %)	Validation cohorts (*N* = 544, %)	*p*-value
Age			
<60	283 (51.8)	296 (54.4)	0.777
≥60	263 (48.2)	248 (45.6)	
AJCC stage			
Stage I	78 (14.3)	103 (18.9)	0.827
Stage II	324 (59.3)	298 (54.8)	
Stage III	123 (22.5)	127 (23.3)	
Stage IV	12 (2.2)	10 (1.8)	
T stage			
T1	127 (23.3)	152 (27.9)	0.881
T2	326 (59.7)	305 (56.1)	
T3	70 (12.8)	67 (12.3)	
T4	20 (3.7)	20 (3.7)	
N stage			
N0	256 (46.9)	258 (47.4)	0.721
N1	178 (32.6)	182 (33.5)	
N2	53 (9.7)	67 (12.3)	
N3	47 (8.6)	29 (5.3)	
M stage			
M0	527 (96.5)	538 (98.9)	0.155
M1	12 (2.2)	1 (0.2)	
ER			
Negative	120 (22.0)	117 (21.5)	0.968
Positive	399 (73.1)	404 (74.3)	
PR			
Negative	168 (30.8)	175 (32.2)	0.878
Positive	349 (63.9)	345 (63.4)	
HER2			
Negative	277 (50.7)	282 (51.8)	0.784
Positive	78 (14.3)	86 (15.8)	
IHC subtype			
Luminal-type	409 (74.9)	411 (75.6)	0.909
HER2-type	17 (3.1)	20 (3.7)	
Basal-type	59 (10.8)	56 (10.3)	

Abbreviations: AJCC, American joint committee on cancer; ER, estrogen receptor; HER2, human epidermal growth factor receptor 2; IHC, immunohistochemistry; PR, progesterone receptor.

Then we identified the prognostic genes from these 96 DE-SRRGs. In the training cohort, univariate Cox regression analysis revealed that six genes were associated with OS (Figure 5A,B). The expressions of EIF2AK3, EIF4EBP1, and HSPA8 were significantly higher in tumor samples than in normal tissues, while ADM, JUN, and SLC38A2 were relatively lower in tumor samples (Figure 5C).

Next, lasso followed by multivariate Cox regression analysis was conducted to construct a prognostic model (Figure 5D). Eventually, an optimal three-gene signature (EIF2AK3, EIF4EBP1, and HSPA8) was identified based on both stepwise strategy. Based on these three genes, we developed the SRRG prognostic signature and computed the risk score for each sample. Patients were classified into higher-risk ($n = 273$) or lower-risk ($n = 273$) groups (Table S14).

In the training cohort, the PCA revealed that the model could separate the higher-risk and lower-risk categories into different groups (Figure 5E). Patients in the higher-risk category had a higher number of deaths (Figure 6A,B). Individuals within the lower-risk category had a better median OS (Figure 6C). In addition, the AUC of the ROC curve reached 0.706 in 1 year and 0.679 in 3 years (Figure 6D). Then, the risk score and other clinicopathological indicators were combined to build a nomogram (Figure 7A). The calibration curve revealed that the signature of SRRG had a high degree of consistency with the actual 3- and 5-year OS (Figure 7B).

3.4 | Validation of the starvation response-related gene signature

Based on the cut-off value identical to that of the training cohort, the individuals in the validation cohort were split into higher-risk ($n = 260$) and lower-risk ($n = 284$) categories (Table S15). Similarly, PCA indicated that the model could divide the higher-risk and lower-risk categories into different groups (Figure 5F). The death rate of samples in the higher-risk class was much higher in the validation cohort (Figure 6E,F). Patients in the lower-risk category presented better OS (Figure 6G), and the ROC curve indicated that the signature had a good prognostic value (Figure 6H), which implied that this SRRG signature was efficacious. According to the calibration curve, this prognostic signature exhibited sound agreement between the estimate of the nomogram and the real statement to forecast the periods of OS at 3 and 5 years in the validation cohort (Figure 7C). In the same way, all findings were presented similarly in the whole cohort (Figure S2A–F).

3.5 | The independent prognostic significance of the starvation response-related gene signature

Univariate Cox regression analysis revealed that the risk score was significantly correlated with OS in training (Figure 8A), validation (Figure 8B), and entire (Figure S3A) cohorts. In multivariate Cox regression analysis, the risk score is still an independent factor of OS after adjusting for additional variables (Figure 8C,D and Figure S3B). In conclusion, the risk score of the prognostic signature we constructed could function as an independent prognostic indicator for BRCA.

3.6 | Establishment of the coexpression networks

The SRRG–ARG coexpression network was created to demonstrate the SRRGs and their connections to ARGs. The network comprised 42 gene pairs (Figure 9A). Further, the SRRG–GRG coexpression network comprised 40 gene pairs (Figure 9B). It is obvious that EIF2AK3 is always located at the core of Figure 9A,B.

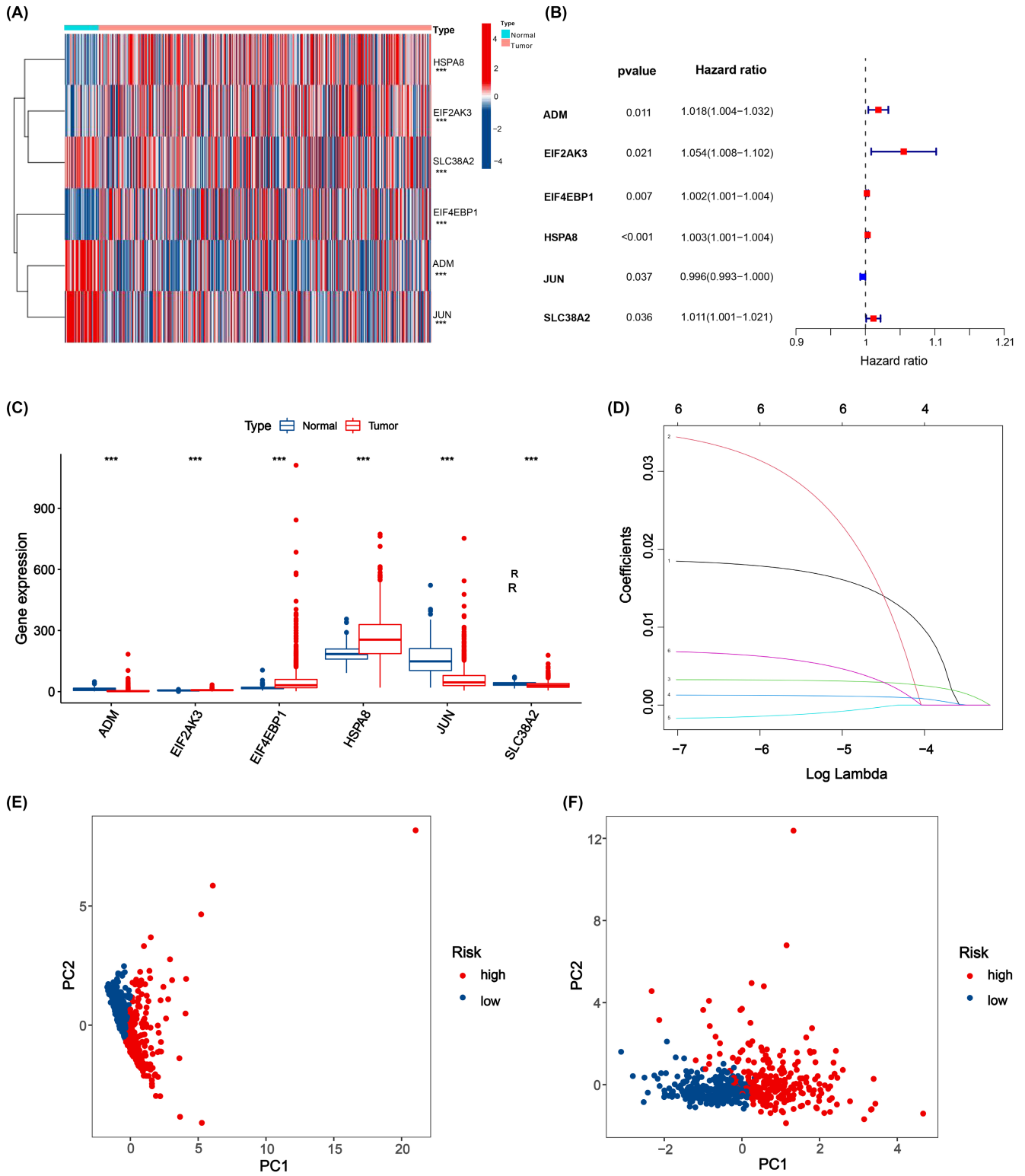

FIGURE 5 The construction of the starvation response-related gene (SRRG) signature. (A) The heatmap revealed six differentially expressed SRRGs associated with overall survival. Forest plot (B) and boxplot (C) of six genes. (D) The SRRG signature was then constructed by lasso regression analysis. Principal component analysis showed the scattered distribution of patients in the training (E) and validation (F) cohorts.

3.7 | Discovery of important hallmarks and functional analysis

Gene set enrichment analysis demonstrated that metabolic-related hallmarks, such as glycolysis, and mTORC1 signaling related to the cancer were upregulated in the higher-risk patients (Figure 10A). In addition, several typical pathways from the KEGG, including the citrate cycle TCA cycle, alanine aspartate, and glutamate metabolism, were highly enriched in high-risk phenotypes (Figure 10B). GO enrichment analysis indicated that genes were remarkably

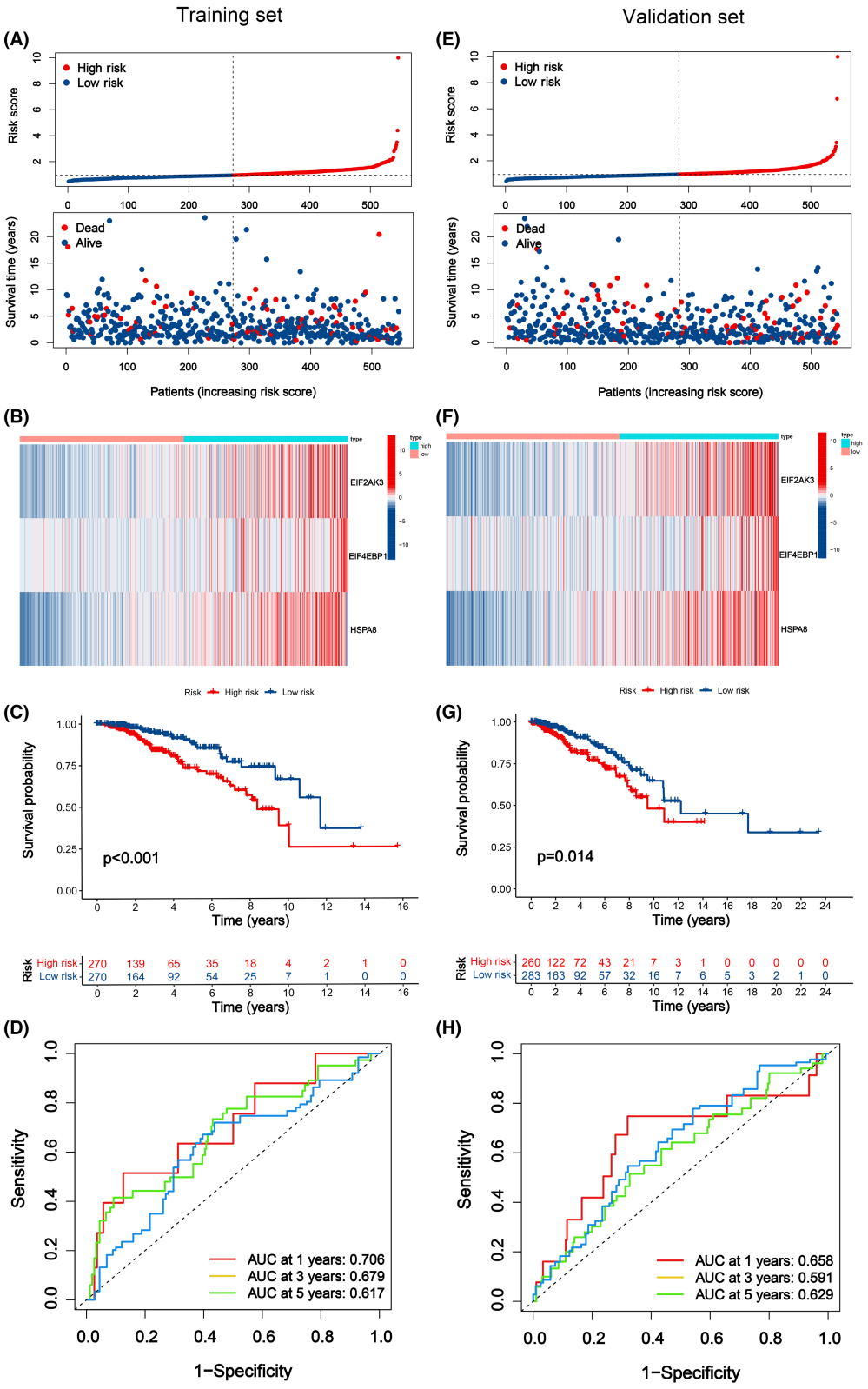

FIGURE 6 Prognostic analysis of the starvation response-related gene signature in the training and validation cohorts. (A, E) The distribution of the overall survival status and the risk score. (B, F) The heatmap depicted the three-gene expression level of each patient. (C, G) Kaplan-Meier curves for the overall survival of patients. (D, H) Area under the curve of time-dependent receiver-operating characteristic curves verified the prognostic accuracy of the signature.

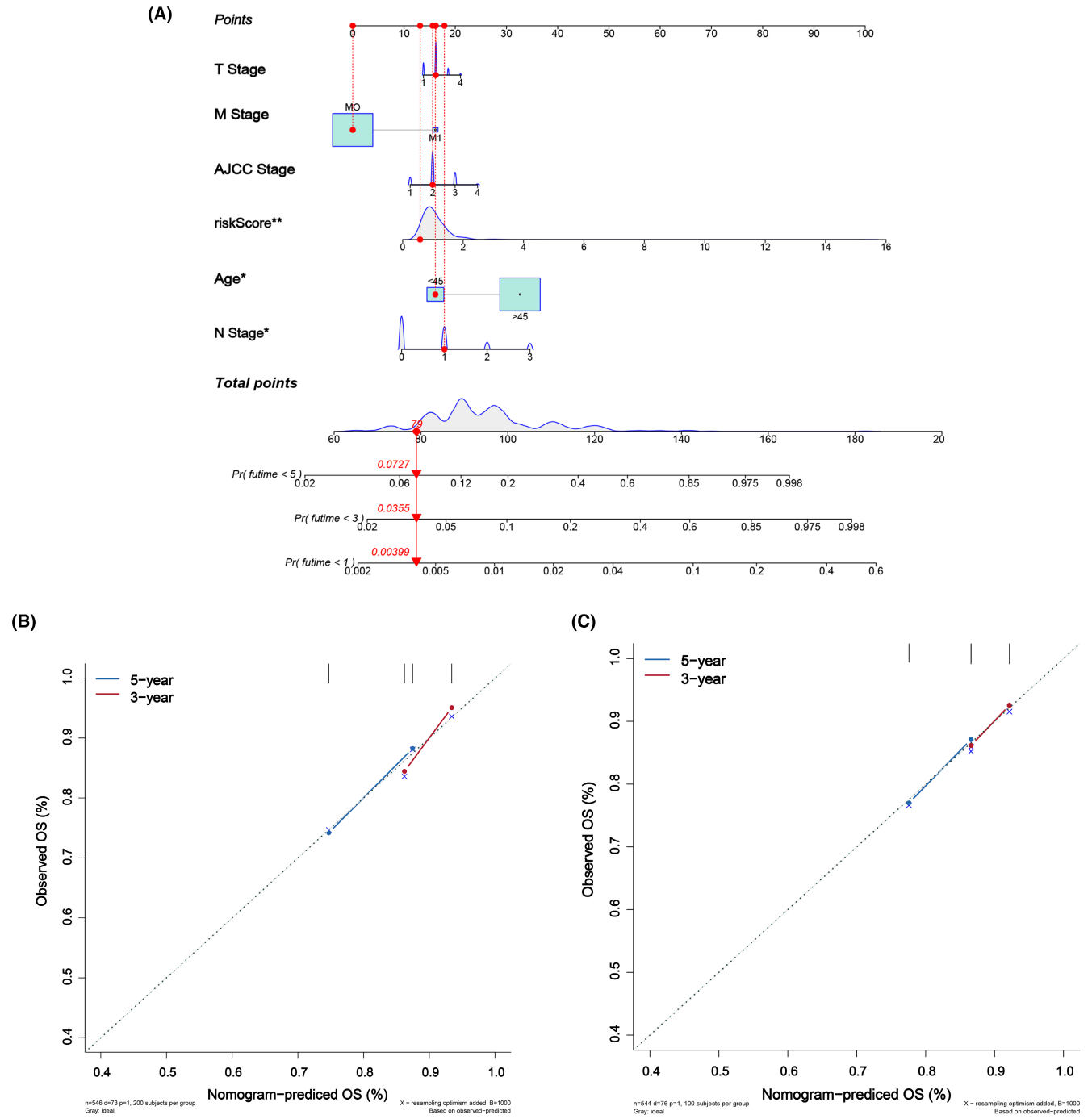

FIGURE 7 Establishment of the nomogram. (A) A nomogram was established by integrating traditional clinicopathological indicators and the risk score. Calibration plots for 3- and 5-year overall survival in training (B) and validation (C) cohorts.

enriched in metabolic-related cellular components, such as mitochondrial matrix, mitochondrial inner membrane, mitochondrial protein-containing complex, and endoplasmic reticulum lumen. Energy stress-related biological processes were also considerably enhanced, such as the response to nutrient levels, and regulation of autophagy (Figure 10C).

3.8 | Inhibition of EIF2AK3 signaling attenuates breast cancer cell invasion and migration in the starved microenvironment

Since EIF2AK3 is always located at the core of Figure 9A,B, we focused on the gene EIF2AK3 for further exploration. As illustrated in

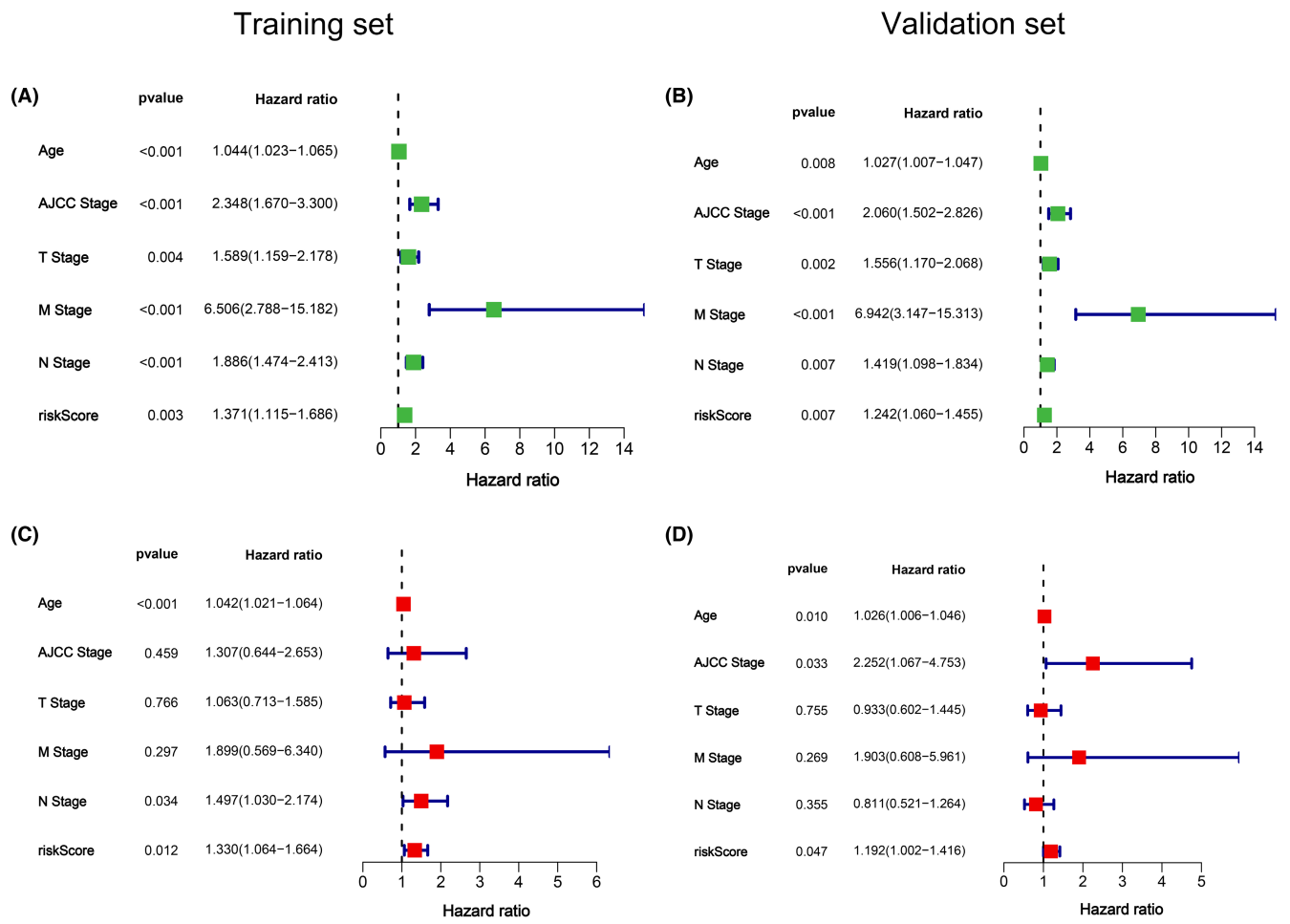

FIGURE 8 The independent prognostic value of the starvation response-related gene signature. Results of univariate and multivariate Cox regression analyses in training (A, C) and validation (B, D) cohorts.

Figure 11A, the mRNA expression level of EIF2AK3 was relatively higher in breast cancerous tissues.

We then also detected changes in phosphorylated EIF2AK3 protein in the starved environment since EIF2AK3 is activated in BRCA by phosphorylation.[9] The protein of the p-EIF2AK3 levels particularly increased in a time-dependent manner in response to starvation stimuli in BRCA cells (Figure 11B,C). In addition, immunofluorescence also showed more elevated levels of p-EIF2AK3 when BRCA cells were in the starved state (Figure 11D,E).

We knocked down EIF2AK3 in MDA-MB-231 and BT549 cells to inhibit EIF2AK3 signaling (Figure 12A,B). The metastatic ability of BRCA cells was lessened after EIF2AK3 was knocked down in the starved environment (Figure 12C,D and Figure S4A,B). Furthermore, inhibition of EIF2AK3 signaling enhanced E-cadherin protein expression while decreasing vimentin and N-cadherin protein expression, implying that EIF2AK3 signaling may participate in the invasive and metastatic potential of BRCA cells in the starved microenvironment through EMT (Figure 12E–H).

4 | DISCUSSION

Fastly expanding tumors frequently suffer from nutritional shortages, and glucose concentrations in tumors are much lower than in the matching normal tissues.[10–13] Solid tumors often develop in nutrient-deficient TME, and energy shortage is especially prevalent due to the high rate of glucose consumption.[4] Neoplastic cells reply to the cytotoxic effects of such metabolic pressures by generating molecular adaptations that enable the clonal selection of a more malignant tumor-initiating cell phenotype.[14,15] The mechanisms underlying cancer cells' adaptation to such fluctuating resource scarcity are the subject of intense research since interfering with adaptive responses might be a practical therapeutic approach.

Cells in solid tumors are subject to severe microenvironmental stresses and must adapt their metabolic processes to overcome multiple unfavorable growth conditions.[16] Increasing evidence indicates that nutrient-deficient microenvironments relate to the development of cancer.[17] For example, it has been shown that

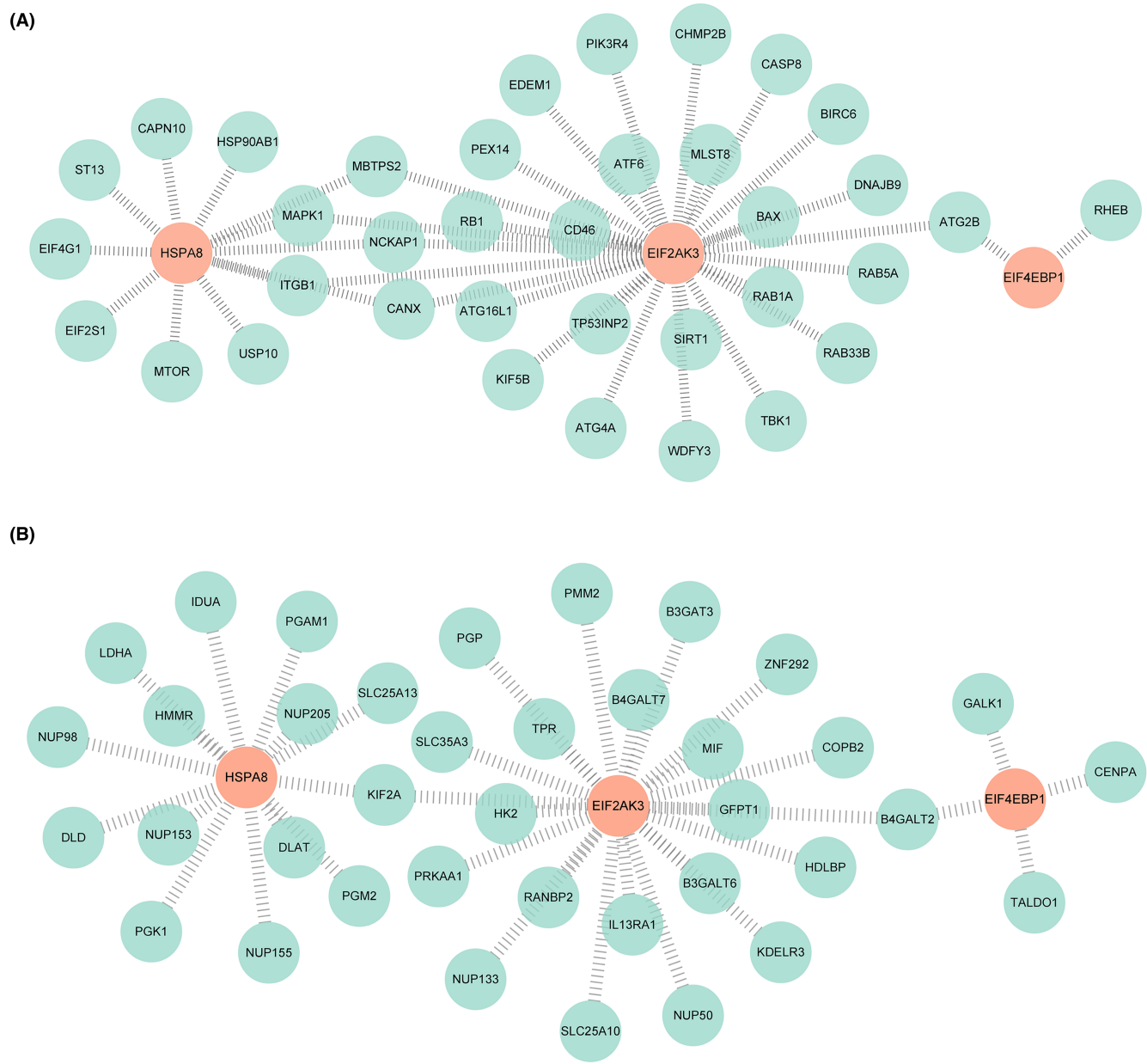

FIGURE 9 Construction of the coexpression networks. The diagrams show the starvation response-related genes (SRRG)–autophagy-related genes (ARG) (A) and starvation response-related gene (SRRG)–glycolysis-related gene (GRG) (B) coexpression network.

glucose-starved tumors are more aggressive.[18] Glucose starvation conditions foster the LKB1 pathway to maintain energy homeostasis and upregulate MMP9 expression, which promotes the metastasis of cancer cells.[19] Loong et al.[14] discovered a regulatory mechanism involving fucosylation through which starvation facilitates cancer stemness, resulting in drug resistance and tumor recurrence. During serum starvation, HCT-8 cells secrete HSP90alpha, which promotes the aggressiveness of colon cancer.[20] Therefore, starvation stimulation is associated with the progression of tumors. However, the biological pertinence and mechanisms of this physiological state in cancer advancement remain evasive and deserve in-depth research.

Starvation induces the autophagic process, which enables the cancer cell to survive by capturing intracellular proteins and reclaiming intracellular elements.[21–23] Starvation induces autophagy in hepatocellular carcinoma cells, which promotes metastasis by activating the Wnt signaling pathway.[5] Autophagy mediated by starvation boosts EMT and the progression of bladder carcinoma through the TGF-signaling pathway.[24] Neoplastic cells trigger autophagy to improve tolerance to nutrient restriction and aid in survival in a deprived microenvironment.[25]

The reprogrammed energy metabolic pattern contributes to the unbounded expansion of neoplastic cells.[26,27] This metabolic phenotype is marked by a prioritized reliance on energy production

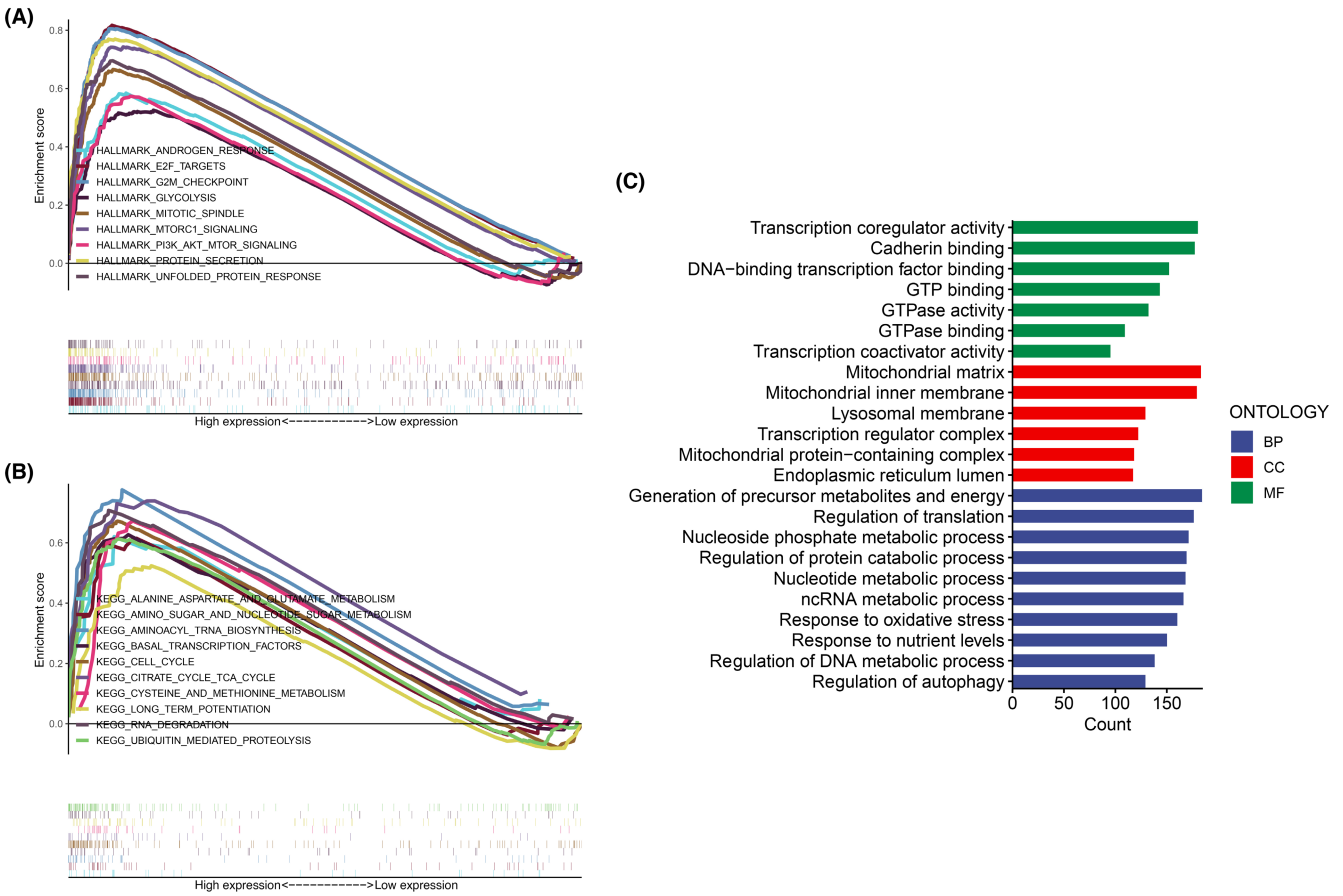

FIGURE 10 Functional enrichment analysis based on the starvation response-related gene signature. (A) Gene set enrichment analysis shows pathways enriched in higher-risk breast cancer patients. (B) Kyoto Encyclopedia of Genes and Genomes shows pathways enriched in the higher-risk group. (C) Gene ontology analysis of differentially expressed genes between high-risk and low-risk groups.

through glycolysis. Our study observed that starved stimulation enhanced the glucose uptake of BRCA cells. Given that protective autophagy of tumor cells could provide substrate for glycolytic pathways and promote glycolysis, we suggest that starvation promotes the glycolytic metabolism in BRCA cells and may be at least partially mediated by protective autophagy. In addition, studies have reported that aerobic glycolysis is triggered when cancer cells are faced with starvation.[16,28–32] Glucose starvation increases the expression levels of key enzymes of glycolysis and accelerates glycolysis, thus maintaining the survival and development of tumor cells in starved environments.[6] Serum starvation upregulates circACC1 to increase glycolysis and promote metabolic adaptation and tumor progression.[33] Amino acid starvation could regulate the production of VEGF, accelerate glucose uptake, and promote glycolysis.[34] Our results show that starvation induces autophagy and glycolytic metabolism, which promotes tumor cell progression.

Massive efforts have been made to exploit noninvasive indicators to forecast early cancer and remind individuals of their cancer risk, which is crucial to reducing BRCA mortality. Since the pathological mechanisms of BRCA advancement are not comprehensively understood, additional investigation is required to recognize and discover practical indicators and targets for BRCA diagnosis and therapy. Recent studies have indicated that mRNA-constructed signatures can anticipate outcomes more precisely.[35–38] So far, limited studies have focused on SRRGs in BRCA. It has not been widely reported in BRCA because the research is still in its early stages. Therefore, we focused on the relationship between SRRGs and BRCA. Our study simulated the starved microenvironment using EBSS and found that starvation stimulation promotes BRCA cell invasion and migration levels. Then, our data indicated that starvation-induced stimulation encourages BRCA cell progression by enhancing autophagy and glucose metabolism. Therefore, using bioinformatics and statistical techniques, we constructed a novel SRRG signature by combining autophagy-related SRRGs and glycolysis-related SRRGs, and we comprehensively examined the precision of the model. The functional enrichment analyses suggested that the SRRGs are closely associated with autophagy and metabolic reprogramming, which promote tumor progression.

Therefore, determining the regulatory molecule in the starved microenvironment of BRCA cells is essential for investigating the specific mechanisms involved. We further analyzed the model core gene EIF2AK3. Interestingly, our experiments revealed that

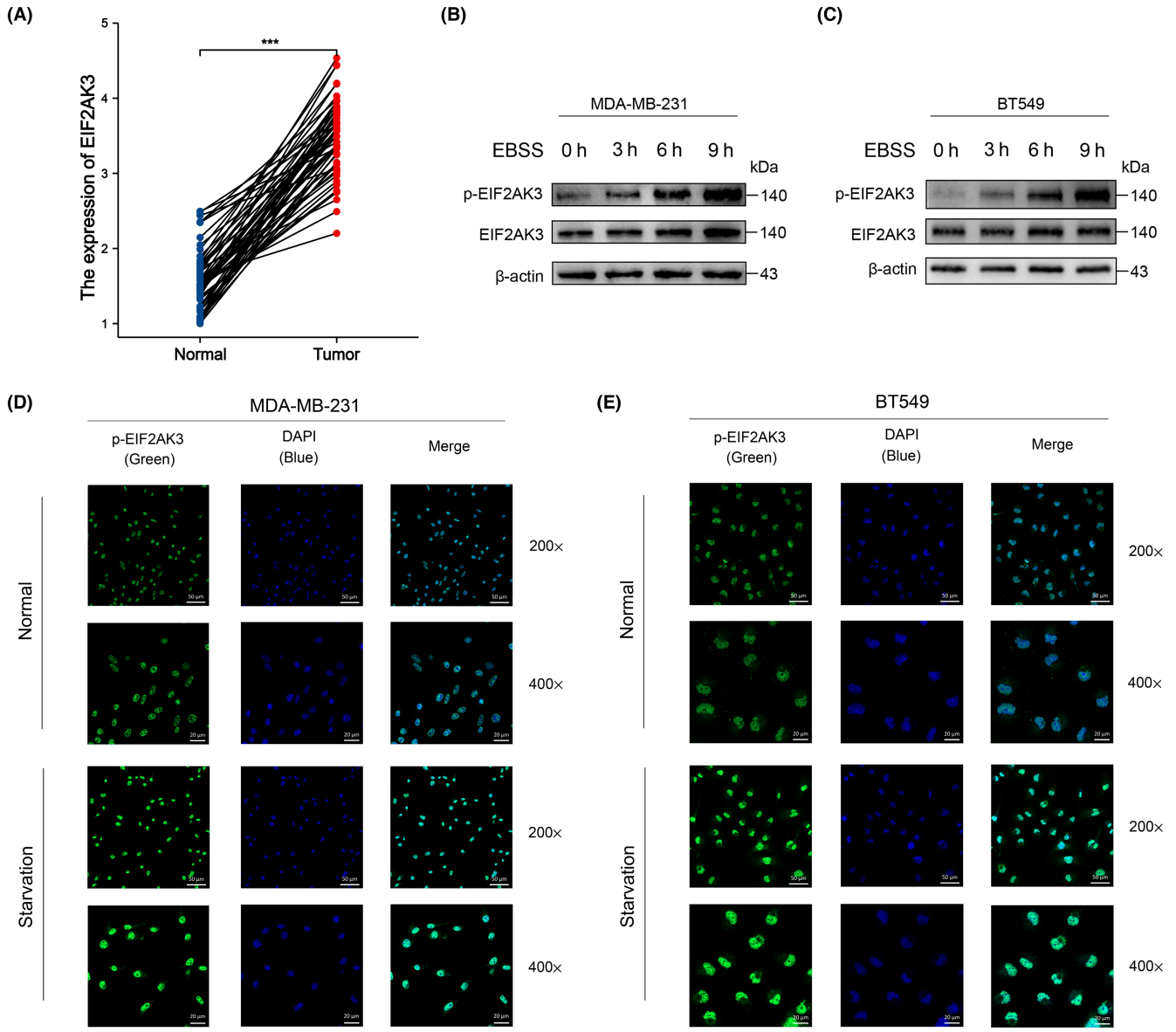

FIGURE 11 EIFA2K3 signaling could be activated by starved stimulation. (A) Quantitative polymerase chain reaction shows the mRNA expression of EIF2AK3 in tissues. (B, C) Western blot showed the p-EIF2AK3 levels in BRCA cells under the starvation environment. (D, E) Immunofluorescence showed the levels of p-EIF2AK3 in BRCA cells under the starvation environment (200× magnification, scale bar represents 50 μm; 400× magnification, scale bar represents 20 μm).

the expression of phosphorylated EIF2AK3 significantly increased after starved stimulation. The invasion and migration capabilities of BRCA cells in starved conditions declined when EIF2AK3 signaling was inhibited. According to research, EIF2AK3 operates during tumor onset and expansion to sustain redox homeostasis and, thus, encourage tumor development.[39] Recent studies suggest EIF2AK3 may drive EMT involvement in triple-negative BRCA (TNBC) metastases.[9,40] These findings indicated that EIF2AK3 is associated with tumor progression, which may be consistent with our speculation that the starved microenvironment promotes BRCA progression via EIF2AK3. Therefore, EIF2AK3 may play a crucial role in the function of the microenvironment of starvation in BRCA.

In conclusion, we identified the SRRGs associated with the prognosis of BRCA and developed a prognostic model. In addition, the starvation response risk score is linked to metabolic-related pathways and biological functions associated with nutritional pressure. As a result, the SRRG signature may have potential prognostic significance and function as a treatment target point for BRCA. Although our analysis utilizes representative and robust data derived from the TCGA public databases, there are still some limitations. First, multicenter studies and additional prospective or retrospective analyses are necessary to verify the role of the SRRG signature that we have proposed. Second, because MDA-MB-231 and BT549 cell lines have a higher invasive migration capacity than other BRCA cell lines and the microenvironment of starvation is an indicator of pro-invasive

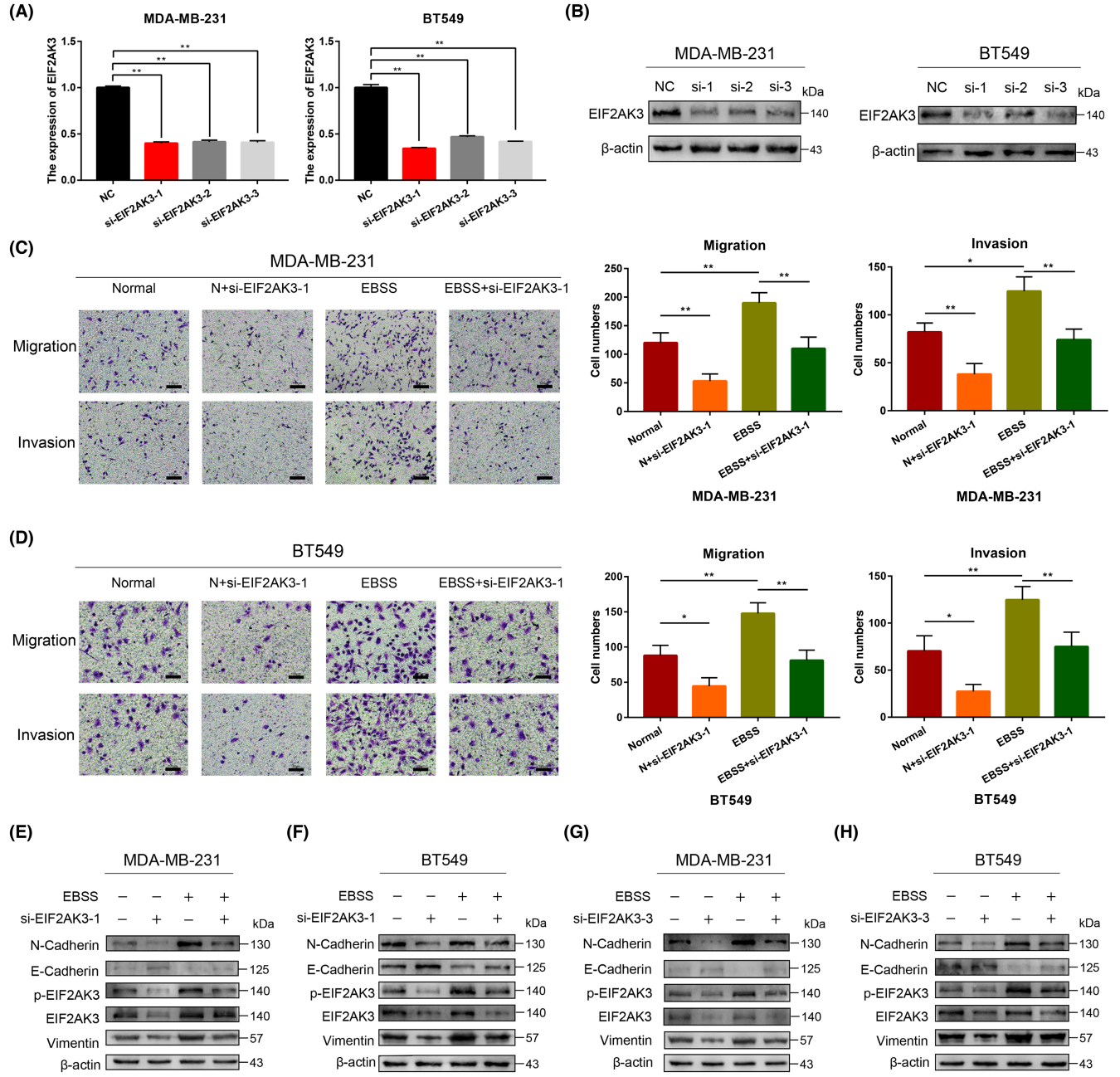

FIGURE 12 Inhibition of EIF2AK3 signaling attenuates breast cancer (BRCA) cell invasion and migration in the starved microenvironment. Quantitative polymerase chain reaction (A) and western blot (B) showed the expression of EIF2AK3 in siRNA-transfected BRCA cells. Transwell assay showed the migration and invasion of MDA-MB-231 (C) and BT549 (D) cells after si-EIF2AK3-1 transfection. The scale bar represents 100 μm. (E–H) Western blot shows the protein expressions of EIF2AK3, p-EIF2AK3, E-cadherin, N-cadherin, and vimentin.

migration, we mainly selected these two types of cells for our study. However, both cell types are TNBC cell lines. Whether EIF2AK3 plays a role in other types of BRCA cells needs to be clarified in future work. Third, since our study preliminarily identified the association between EIF2AK3 and the microenvironment of starvation in BRCA, underlying and potential mechanisms need to be further investigated through experimentation in the future.

AUTHOR CONTRIBUTIONS

YW developed the study concept and design, performed data acquisition and analysis, and drafted the manuscript. SCL obtained funding and supervised the study. YW and YKX performed the bioinformatics and statistical data analyses. SG and ZRT constructed the figures and tables. All authors contributed to the article and approved the submitted version.

FUNDING INFORMATION

This study was funded by the National Natural Science Foundation of China (No. 81772979) and the Doctoral Research Innovation Project of the First Affiliated Hospital of Chongqing Medical University (Grant No. CYYY-BSYJSCXXM-202213).

CONFLICT OF INTEREST STATEMENT

The authors declare that the research was conducted without any commercial or financial relationships that could be construed as a potential conflict of interest.

ETHICS STATEMENT

Approval of the research protocol by an Institutional Review Board: This study was approved by the Institutional Review Board of the First Affiliated Hospital of Chongqing Medical University and conformed to the provisions of the Declaration of Helsinki.

Informed Consent: All patients in this study provided signed informed consent.

Registry and the Registration No. of the study/trial: N/A.

Animal Studies: N/A.

ORCID

Yuan Wang https://orcid.org/0000-0002-7002-0408

Shengchun Liu https://orcid.org/0000-0002-9933-3643

REFERENCES

1. Harbeck N, Penault-Llorca F, Cortes J, et al. Breast cancer. *Nat Rev Dis Primers*. 2019;5(1):66.
2. Gonzalez FJ, Xie C, Jiang C. The role of hypoxia-inducible factors in metabolic diseases. *Nat Rev Endocrinol*. 2018;15(1):21-32.
3. Hamanaka RB, Chandel NS. Cell biology. Warburg effect and redox balance. *Science*. 2011;334(6060):1219-1220.
4. Grasmann G, Smolle E, Olschewski H, Leithner K. Gluconeogenesis in cancer cells – repurposing of a starvation-induced metabolic pathway? *Biochim Biophys Acta Rev Cancer*. 2019;1872(1):24-36.
5. Fan Q, Yang L, Zhang X, et al. Autophagy promotes metastasis and glycolysis by upregulating MCT1 expression and Wnt/β-catenin signaling pathway activation in hepatocellular carcinoma cells. *J Exp Clin Cancer Res*. 2018;37(1):9.
6. Fu LN, Wang YQ, Tan J, et al. Role of JMJD2B in colon cancer cell survival under glucose-deprived conditions and the underlying mechanisms. *Oncogene*. 2018;37(3):389-402.
7. Ashburner M, Ball CA, Blake JA, et al. Gene ontology: tool for the unification of biology. The Gene Ontology Consortium. *Nat Genet*. 2000;25(1):25-29.
8. Kanehisa M, Furumichi M, Sato Y, Ishiguro-Watanabe M, Tanabe M. KEGG: integrating viruses and cellular organisms. *Nucleic Acids Res*. 2021;49(D1):D545-D551.
9. Feng YX, Sokol ES, Del Vecchio CA, et al. Epithelial-to-mesenchymal transition activates PERK-eIF2α and sensitizes cells to endoplasmic reticulum stress. *Cancer Discov*. 2014;4(6):702-715.
10. Hirayama A, Kami K, Sugimoto M, et al. Quantitative metabolome profiling of colon and stomach cancer microenvironment by capillary electrophoresis time-of-flight mass spectrometry. *Cancer Res*. 2009;69(11):4918-4925.
11. Wang L, Chen J, Chen L, et al. 1H-NMR based metabonomic profiling of human esophageal cancer tissue. *Mol Cancer*. 2013;12:25.
12. Ziebart T, Walenta S, Kunkel M, Reichert TE, Wagner W, Mueller-Klieser W. Metabolic and proteomic differentials in head and neck squamous cell carcinomas and normal gingival tissue. *J Cancer Res Clin Oncol*. 2011;137(2):193-199.
13. Rocha CM, Barros AS, Goodfellow BJ, et al. NMR metabolomics of human lung tumours reveals distinct metabolic signatures for adenocarcinoma and squamous cell carcinoma. *Carcinogenesis*. 2015;36(1):68-75.
14. Loong JH, Wong TL, Tong M, et al. Glucose deprivation-induced aberrant FUT1-mediated fucosylation drives cancer stemness in hepatocellular carcinoma. *J Clin Invest*. 2021;131(11):e143377.
15. Roberts HR, Smartt HJ, Greenhough A, et al. Colon tumour cells increase PGE(2) by regulating COX-2 and 15-PGDH to promote survival during the microenvironmental stress of glucose deprivation. *Carcinogenesis*. 2011;32(11):1741-1747.
16. Yun J, Rago C, Cheong I, et al. Glucose deprivation contributes to the development of KRAS pathway mutations in tumor cells. *Science*. 2009;325(5947):1555-1559.
17. García-Jiménez C, Goding CR. Starvation and pseudo-starvation as drivers of cancer metastasis through translation reprogramming. *Cell Metab*. 2019;29(2):254-267.
18. Ma L, Tao Y, Duran A, et al. Control of nutrient stress-induced metabolic reprogramming by PKCζ in tumorigenesis. *Cell*. 2013;152(3):599-611.
19. Endo H, Owada S, Inagaki Y, Shida Y, Tatemichi M. Glucose starvation induces LKB1-AMPK-mediated MMP-9 expression in cancer cells. *Sci Rep*. 2018;8(1):10122.
20. Chen JS, Hsu YM, Chen CC, Chen LL, Lee CC, Huang TS. Secreted heat shock protein 90alpha induces colorectal cancer cell invasion through CD91/LRP-1 and NF-kappaB-mediated integrin alphaV expression. *J Biol Chem*. 2010;285(33):25458-25466.
21. Viry E, Paggetti J, Baginska J, et al. Autophagy: an adaptive metabolic response to stress shaping the antitumor immunity. *Biochem Pharmacol*. 2014;92(1):31-42.
22. Thomas M, Davis T, Loos B, et al. Autophagy is essential for the maintenance of amino acids and ATP levels during acute amino acid starvation in MDAMB231 cells. *Cell Biochem Funct*. 2018;36(2):65-79.
23. Amaravadi R, Kimmelman AC, White E. Recent insights into the function of autophagy in cancer. *Genes Dev*. 2016;30(17):1913-1930.
24. Tong H, Yin H, Hossain MA, et al. Starvation-induced autophagy promotes the invasion and migration of human bladder cancer cells via TGF-β1/Smad3-mediated epithelial-mesenchymal transition activation. *J Cell Biochem*. 2019;120(4):5118-5127.
25. Sato K, Tsuchihara K, Fujii S, et al. Autophagy is activated in colorectal cancer cells and contributes to the tolerance to nutrient deprivation. *Cancer Res*. 2007;67(20):9677-9684.
26. Warburg O. On the origin of cancer cells. *Science*. 1956;123(3191):309-314.
27. Hanahan D, Weinberg RA. Hallmarks of cancer: the next generation. *Cell*. 2011;144(5):646-674.
28. Sukonina V, Ma H, Zhang W, et al. FOXK1 and FOXK2 regulate aerobic glycolysis. *Nature*. 2019;566(7743):279-283.
29. Li T, Tong H, Yin H, et al. Starvation induced autophagy promotes the progression of bladder cancer by LDHA mediated metabolic reprogramming. *Cancer Cell Int*. 2021;21(1):597.
30. Zhu W, Chen X, Guo X, et al. Low glucose-induced overexpression of HOXC-AS3 promotes metabolic reprogramming of breast cancer. *Cancer Res*. 2022;82(5):805-818.
31. Tang J, Yan T, Bao Y, et al. LncRNA GLCC1 promotes colorectal carcinogenesis and glucose metabolism by stabilizing c-Myc. *Nat Commun*. 2019;10(1):3499.
32. Sun L, Song L, Wan Q, et al. cMyc-mediated activation of serine biosynthesis pathway is critical for cancer progression under nutrient deprivation conditions. *Cell Res*. 2015;25(4):429-444.
33. Li Q, Wang Y, Wu S, et al. CircACC1 regulates assembly and activation of AMPK complex under metabolic stress. *Cell Metab*. 2019;30(1):157-173.e7.

34. Longchamp A, Mirabella T, Arduini A, et al. Amino acid restriction triggers angiogenesis via GCN2/ATF4 regulation of VEGF and H2S production. *Cell*. 2018;173(1):117-129.e14.
35. Jiang C, Liu Y, Wen S, Xu C, Gu L. In silico development and clinical validation of novel 8 gene signature based on lipid metabolism related genes in colon adenocarcinoma. *Pharmacol Res*. 2021;169:105644.
36. Zhou C, Zhao Y, Yin Y, et al. A robust 6-mRNA signature for prognosis prediction of pancreatic ductal adenocarcinoma. *Int J Biol Sci*. 2019;15(11):2282-2295.
37. Li X, Dai Z, Wu X, et al. The comprehensive analysis identified an autophagy signature for the prognosis and the immunotherapy efficiency prediction in lung adenocarcinoma. *Front Immunol*. 2022;13:749241.
38. Zhang L, Zhang Z, Yu Z. Identification of a novel glycolysis-related gene signature for predicting metastasis and survival in patients with lung adenocarcinoma. *J Transl Med*. 2019;17(1):423.
39. Bobrovnikova-Marjon E, Grigoriadou C, Pytel D, et al. PERK promotes cancer cell proliferation and tumor growth by limiting oxidative DNA damage. *Oncogene*. 2010;29(27):3881-3895.
40. Feng YX, Jin DX, Sokol ES, Reinhardt F, Miller DH, Gupta PB. Cancer-specific PERK signaling drives invasion and metastasis through CREB3L1. *Nat Commun*. 2017;8(1):1079.

SUPPORTING INFORMATION

Additional supporting information can be found online in the Supporting Information section at the end of this article.

How to cite this article: Wang Y, Gao S, Xu Y, Tang Z, Liu S. Characterization of starvation response-related genes for predicting prognosis in breast cancer. *Cancer Sci*. 2023;114:3144-3161. doi:10.1111/cas.15836